IEEE Access
Multidisciplinary ⋮ Rapid Review ⋮ Open Access Journal

Received December 6, 2019, accepted December 23, 2019, date of publication December 26, 2019, date of current version January 7, 2020.

Digital Object Identifier 10.1109/ACCESS.2019.2962530

Output Voltage Control of BESS Inverter in Stand-Alone Micro-Grid Based on Expanded Inverse Model

XINGWU WANG[1,2], YONGJUN LIN[1], BINGSHU WANG[1,2], WEILIANG LIU[1], AND KANG BAI[1]

[1]School of Control Science and Engineering, North China Electric Power University, Baoding 071003, China
[2]Baoding Sinosimu Technology Company, Ltd., Baoding 071051, China

Corresponding author: Weiliang Liu (51651798@ncepu.edu.cn)

This work was supported by the Fundamental Research Funds for the Central Universities under Grant 2019MS100 and Grant 2017MS134.

ABSTRACT This paper investigates robust output voltage control of battery energy storage systems (BESS) inverter in stand-alone micro-grid. The transfer function model between the output voltage and duty cycle of the BESS inverter is established, base on which the main factors affecting the output voltage are analyzed theoretically. Then, the expanded inverse model of the BESS inverter is developed based on BP neural network, and the gravity search algorithm (GSA) is employed to search the initial values of the network's parameters in the training process. Further, a control method for the output voltage of BESS inverter is proposed by putting the expanded inverse model in series with the original system as well as performing the single-loop control with PI controller. Both simulation experiment results and prototype experiment results show that the proposed expanded inverse model control method has a strong capability of disturbance rejection and could ensure the high power quality for the output voltage of the BESS inverter.

INDEX TERMS BESS inverter, inverse model, BP neural network, gravity search algorithm, load disturbance.

I. INTRODUCTION

Microgrids are the systems that integrate renewable-energy sources (RESs), energy storage systems (ESS) and loads on a low-voltage network which can operate in either grid-connected mode or stand-alone mode [1], [2], [3]. The stability of voltage, which means the power balance between supply and demand, is one of the most important power quality issues for the microgrid. In the grid-connect mode, the microgrid voltage is maintained within a tight range by the main grid. In the stand-alone mode, however, the achievement of stable microgrid voltage is not straightforward [4]. Power unbalance between supply and demand would cause the microgrid voltage to fluctuate, and the system can even experience a blackout if no prevention measures are considered [5], [6].

The battery energy storage systems (BESS), an ESS which is composed of storage batteries and a power electronic device, inverter, has a faster response speed to release energy than general ESS [7], [8]. Therefore, in stand-alone mode microgrid, BESS usually works as the main power source to provide stable system voltage, thereby overcome the internal power unbalance between RES and loads [9], [10]. Compared with general inverters, the voltage control of the BESS inverter is more challenging for large-scale variation of the operating point and frequent disturbance [11]. Therefore, a voltage control method with strong disturbance-rejection capability, low harmonic voltage content is expected for the BESS inverter.

In existed studies, different control methods for inverters have been proposed, such as PI control method, hysteresis control method, dead-beat control method and proportional resonant (PR) control method [12]. The PI control method is commonly used in inverter applications, generally, the switching frequency is a constant which could simplify the filter design. Unfortunately, it is hard to track a sinusoidal reference without steady-state error and also has poor adaptability to the load disturbance [13].

Hysteresis control method generates the triggering pulses for the switches directly based on the detection of the control

The associate editor coordinating the review of this manuscript and approving it for publication was Yonghao Gui.

error, which has the virtues of simplicity and robustness, however, the achievable minimum error value is twice the hysteresis band, and the variable switching frequency is disadvantageous to the filter design [14], [15].

Dead-beat control method can ensure a fast dynamic response and also a precise compensation of any disturbance [16], [17]. However, the variations of passive elements values, and the control time delay, have an obvious influence on the performance of this control method, sometimes may cause the instability of the system.

PR control method could eliminate the steady-state error at a certain frequency through the introduction of an infinite gain at resonant frequency [18], [19]. However, only low-order voltage harmonics could be eliminated for the sake of system instability when the compensated frequency beyond the bandwidth of the system.

Self-adaptive inverse control method has drawn much attention in engineering applications owing to the clear physical concept, being intuitive and easy to understand [20], [21]. However, the accurate model of the original system should be acquired in advance, which is quite difficult to meet in practice. Furthermore, even if the accurate model of the original system was acquired, it is often quite difficult to solve the inverse model [22]. At the same time, artificial neural networks (ANNs) have been widely applied in modeling and control of complex dynamic systems with impressive adaptive learning capability and strong fault tolerance ability [23]. Combining them, the inverse control method based on ANN-model could overcome the difficulty of solving the inverse problem, thus showing a promising future in applications. In recent years, ANN-model based inverse control method has been applied in different fields [24], [25], [26].

It is unfortunate in the literature that few reports describe the application of the inverse model control method to the BESS inverter. In the previous work of the authors [27], aiming at improving the BESS inverter's adaptability to the disturbance in stand-alone micro-grid, an inverse model of BESS inverter is established using BP neural network, and the simulation result show that inverse control method could effectively improve the dynamic response speed and reduce the harmonic content of the inverter output voltage. This paper could be considered as the extension and improvement of the literature [27], the main contributions are as follows:

(1) The transfer function model between the output voltage and duty cycle of the BESS inverter is established, based on which the main factors affecting the output voltage are analyzed theoretically.

(2) The inverse model of the BESS inverter is constructed based on BP neural network, of which the initial values of network's parameters is determined by the gravity search algorithm (GSA) in the training process.

(3) An output voltage control method for BESS inverter is proposed by putting the expanded inverse model in series with the original system as well as performing the single-loop control with PI controller, and the effectiveness of the control method is validated by simulation.

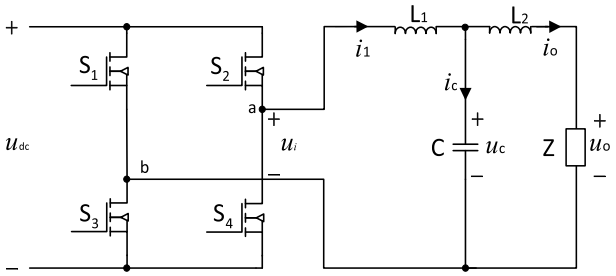

FIGURE 1. Topology of single-phase BESS inverter.

TABLE 1. Component parameters of the BESS inverter.

Parameter name	Parameter value
Filter inductance L_1	4.7 mH
Filter capacity C	6.8 uF
Filter inductance L_2	1.2 mH
BESS port voltage u_{dc}	400 V
Inverter output voltage u_o	220 V
Inverter raged power P	10 kW

(4) A prototype of a BESS inverter is developed, based on which the effectiveness of the proposed control method is further validated.

Accordingly, contents of this paper include seven parts: Model of the BESS inverter (Section 2); Structure of the inverse model of the BESS inverter (Section 3); Training of the neural network inverse model (Section 4); Design of the inverse control scheme (Section 5); Simulation experiment (Section 6); Prototype experiment (Section 7); Conclusion (Section 8).

II. MODEL OF BESS INVERTER

A typical single-phase BESS inverter is depicted in Fig.1. It is known that the system consists of a DC–AC voltage source inverter and an LCL filter. The LCL filter is employed to reduce the high-frequency harmonic components in the waveform of voltage u_o. Z is the equivalent load in stand-alone mode microgrid, the consume power of which is equal to the power difference between the load and RESs. Assume u_{dc} is the port voltage of BESS, d is the duty cycle of the PWM generator that works in unipolar method, u_i is the output voltage impulse sequence of the voltage source inverter, u_{iA} is the mean value of u_i, when the switching frequency of the inverter is fast enough, there is $d = u_{iA}/u_{dc}$.

Take inductor current i_1, inverter output current i_o and capacitor voltage u_c as state variables, the state equations of the system depicted in Fig.1 are

$$\frac{di_1}{dt} = -\frac{u_c}{L1} + \frac{u_i}{L1} \tag{1}$$

$$\frac{di_o}{dt} = -\frac{Zi_o}{L2} + \frac{u_c}{L2} \tag{2}$$

$$\frac{du_c}{dt} = \frac{i_1}{C} - \frac{i_o}{C} \tag{3}$$

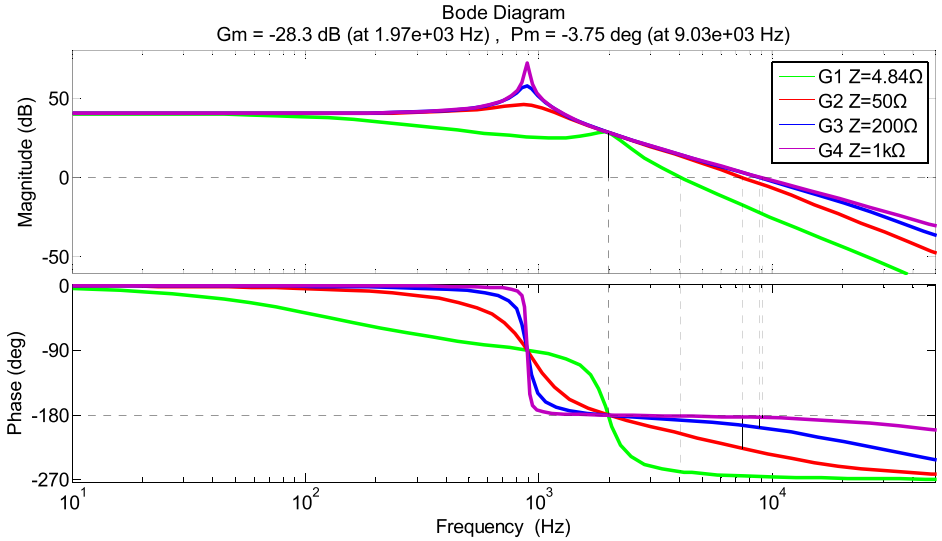

FIGURE 2. Bode diagram of the BESS inverter under different equivalent load.

$$\begin{bmatrix} \dot{i}_1 \\ \dot{i}_o \\ \dot{u}_c \end{bmatrix} = \begin{bmatrix} 0 & 0 & -\frac{1}{L_1} \\ 0 & -\frac{Z}{L_2} & \frac{1}{L_2} \\ \frac{1}{C} & -\frac{1}{C} & 0 \end{bmatrix} \begin{bmatrix} i_1 \\ i_o \\ u_c \end{bmatrix} + \begin{bmatrix} \frac{1}{L_1} \\ 0 \\ 0 \end{bmatrix} u_i \quad (4)$$

$$u_o = [0 \quad Z \quad 0] \begin{bmatrix} i_1 \\ i_o \\ u_c \end{bmatrix} \quad (5)$$

The transfer function $G(s)$ between inverter output voltage u_o and duty cycle d could be obtained by small-signal modeling method as [28]:

$$G(s) = \frac{u_{dc} Z L_2}{L_1^2 L_2 C s^3 + Z C L_1^2 s^2 + (L_1^2 + L_1 L_2) s + L_1 Z} \quad (6)$$

According to the mathematical model of the BESS inverter, the main factors affecting the inverter output voltage u_o mainly include the following variables:

(1) Equivalent load Z. When Z is a linear load like RLC type load, the inverter has a linear characteristic, however, the inverter stability is unlike under different Z. The typical component parameters of a 10kW BESS inverter are shown in Tab.1, of which the LCL filter is designed to reduce the switching frequency ripple while has the characteristics of rapid dynamic response and good stability margin [29], [30]. Take resistor type load as an example, the inverter bode diagram under different Z is shown in Fig.2 according to the component parameters in Tab.1. It is known that the phase margin is negative, which means the inverter is unstable, and a heavier Z matches a smaller phase margin. When Z is a non-linear load, the inverter has a corresponding nonlinear characteristic. Rectifier type load is the most common nonlinear load, the turn on and turn off process can be regarded as the periodic switching of no-load and equivalent heavy load, therefore, it is easy to distort the inverter output voltage [31]. Because inverter output current i_o could reflect the change of Z, it could be taken as a disturbance of the BESS inverter output voltage u_o.

(2) BESS port voltage u_{dc}. u_{dc} represents the state of charge (SOC) for BESS, which varies on a large scale along with the change of working conditions. From Eq. (6), it is known that u_{dc} directly affects the gain of the transfer function $G(s)$, and in further affects the steady-state value of the inverter output voltage u_o. Therefore, u_{dc} should be taken into account for the control of inverter output voltage.

(3) Capacitor voltage u_c. u_c is the system state variable which reflects the internal state of the LCL filter, thus influence the dynamic process of the output voltage of the inverter.

(4) Duty cycle d. d is the control input of the inverter which directly affects the steady-state value of the output voltage of the inverter.

III. STRUCTURE OF INVERSE MODEL OF BESS INVERTER

A. PRINCIPLE OF NEURAL NETWORK INVERSE MODEL

It is known from neural network inverse system theory that if the inverse model $u = f^{-1}(y)$ of a typical SISO nonlinear system $y = f(u)$ can be approximated by a neural network model and this model is put in series with the original system, then a pseudo-linear system $y = g(y^*)$ can be constructed and solved with conventional linear system methods. As shown in Fig.3, the input of this kind of NN inverse model only includes the control input, therefore, it is called the basic-structure inverse system model [21].

To make full use of the information of the original system, and enhance the anti-disturbance capability of the inverse system model, some important state variables and disturbances of the original system could be added to the inputs of the basic-structure neural network inverse system model. As a result, an expanded neural network inverse system model could be constructed, as shown in Fig.4. After the expanded

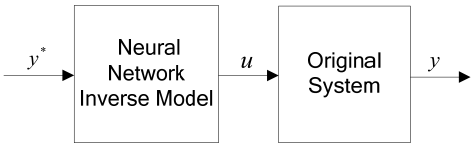

FIGURE 3. Basic structure of the neural network inverse system.

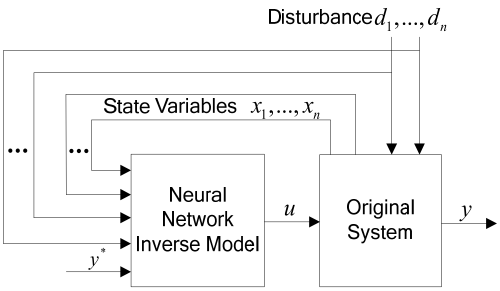

FIGURE 4. Structure of the expanded inverse model.

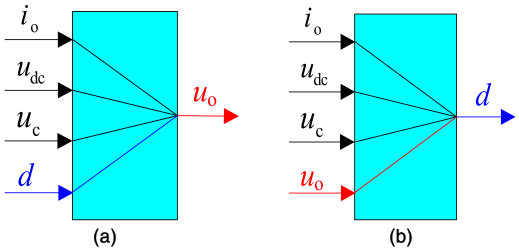

FIGURE 5. Direct/inverse models for the output voltage of a BESS inverter. a) Direct model; b) Inverse model.

neural network inverse system model has been established, trained and validated with high precision, a neural network inverse control method could be designed to realize inverse control of the original system.

B. STRUCTURE OF THE INVERSE MODEL

It is known from the analysis in Section 2 that the main factors affecting the inverter output voltage u_o includes BESS port voltage u_{dc}, inverter output current i_o, capacitor voltage u_c, and duty cycle d, therefore, direct model for the inverter output voltage u_o could be set up as shown in Fig.5 a), while the inverse model could be formed as shown in Fig.5 b).

In this study, digital control mode is considered in the implementation of the BESS inverter control. For the kth control period of the BESS inverter, assume the sampling of BESS port voltage $u_{dc}(k)$, capacitor voltage $u_c(k)$, inverter output current $i_o(k)$, inverter output voltage $u_o(k)$ is performed at the beginning of the control period, meanwhile, duty cycle of the PWM generator $d(k)$ is generated. Therefore, for direct model, $u_{dc}(k)$, $u_c(k)$, $i_o(k)$ and $d(k)$ should be taken as inputs, and the output is the sampling of inverter output voltage in $k+1$th control period, $u_o(k+1)$. To represent the inverter dynamic characteristic more accurately, the duty cycle $d(k\text{-}1)$ of k-1 th control period, the inverter output current $i_o(k\text{-}1)$ of k-1th control period, and $u_o(k)$ could be

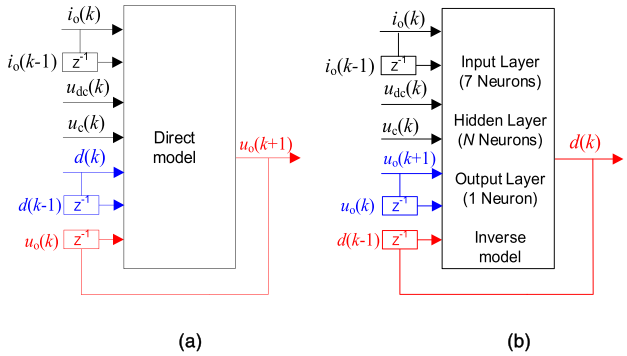

FIGURE 6. Structure of direct/inverse models for the output voltage of a BESS inverter. a) Direct model; b) Inverse model.

added in the inputs of the direct model, as shown in Fig.6 a). The direct model has 7 inputs and 1 output, correspondingly, a BP neural network inverse model could be constructed as shown in Fig.6 b), which has 7 neurons in the input layer, 1 neuron in the output layer, and N neurons in the hidden layer.

IV. TRAINING OF NEURAL NETWORK INVERSE MODEL

A. DATA COLLECTION

The BP neural network inverse model should be trained with the sample data set after the models' inputs, outputs and structures are determined. To make a neural network model fully represent the dynamic and static characteristics of the controlled object, the training data should be rich enough to contain different operating conditions under which the model will be applied. In this work, a BESS inverter model is built with Matlab to collect the sample data set.

For Simscape in Simulink environment of Matlab, both the inside Power system libraries and Electronics libraries could be used to model an electrical system, however, Electronics libraries provide more detailed blocks, which are more suitable for high-precision modeling. Therefore, Electronics libraries are chosen to build the BESS inverter model according to the parameters of Tab.1.

During the collection of data sets, different inverter operating conditions are considered. The BESS inverter runs with a conventional PI control method, and the control period is 10^{-4}s according to the PWM switching frequency of 10 kHz. 63 kinds of different equivalent load in total are taken into account, including linear equivalent load, nonlinear equivalent load, and equivalent load switching, as shown in Tab.2. Meanwhile, to reflect the influence of SOC variation, when collecting samples under every kind of equivalent load, the initial value of port voltage u_{dc} is randomly given between 350V and 450V. 25200 sets of data are collected in total, randomly select 22200 of them as training data set, and the remain 3000 of them as test data set, then Matlab Neural Network Toolbox is used to train the inverse models.

B. TRAINING OF INVERSE MODEL

Generally, the number of hidden nodes N as well as the activation functions in a neural network has an obvious influence on

TABLE 2. Working conditions for the collection of data sets.

Working conditions	Equivalent load type	Number of types	Equivalent load Power (ratio to rated power of BESS inverter)		
Linear equivalent load	Resistor load	5	10%, 25%, 50%, 75%, 100%		
Nonlinear equivalent load	Resistor load+ Rectifier load	50	Resistor load: 25%	Rectifier load: 25%, 50%, 75%	Conducting angle:15°, 30°, 45°, 60°, 75°
			Resistor load: 50%	Rectifier load: 25%, 50%	
			Resistor load: 75%	Rectifier load: 25%	
			———	Rectifier load: 25%, 50%, 75%, 100%	
Equivalent load switching	Resistor load	8	no load-full load; full load-no load; load increase: 10%, 25%, 50%; load decrease: 100%, 75%, 50%		

its performance. The optimal scope of N could be calculated as [3,12] according to the following empirical formula:

$$N = \sqrt{m+n} + \alpha \tag{7}$$

where m is the number of neurons in the input layer, n is the number of neurons in the output layer, and α is the integer number belongs to [1,10]. In this paper, the optimal N are determined by trial and error, that is, the activation functions of the hidden layer and the output layer adopt sigmoid function and purelin function respectively, the inverse model is directly trained with standard BP algorithm for 1000 cycles, and the mean squared errors (MSEs) for 10 times of training are shown in Tab.3, it is known that the optimal N is 9 for minimum MSE is achieved.

There are three kinds of activation functions in Matlab Neural Network Toolbox, sigmoid function, tansig function, and purelin function. The performance of the neural network under different conditions of activation functions are further investigated, as shown in Table.4, it is known that smaller MSEs are achieved when the activation function of hidden layer is chosen to be sigmoid or tansig, while the activation function combination of sigmoid-purelin achieves the minimum MSE.

The minimum MSE is not quite ideal for the training process is generally easy to fall into local optimization due to the random selection of initial network parameters like connection weights and thresholds for the neurons. In order to avoid this phenomenon, the gravitational search algorithm (GSA) is employed to search the optimal initial value of the network's parameters in this study.

Gravitational search algorithm (GSA) is a nature-inspired metaheuristic optimization method firstly proposed by Rashedi et al. in 2009, of which the basis is Newton's second law of motion [32]. In GSA, searcher agents are considered being individual objects attracting each other by gravitational force, and the masses of the objects are assigned according to their evaluation value. The gravitational force causes the movement of all objects towards the sub-optimum solutions. Consequently, the heavier objects correspond to better solutions while lighter objects correspond to the weaker solutions of the problem.

In the search space, each solution is presented by the position vector of each object and can be defined by

$$P_i = (p_i^1, \ldots, p_i^d, \ldots, p_i^D) \text{ for } i = 1, 2, 3, \ddot{y}, N_1, \tag{8}$$

The position of the object i in the d-th dimension is presented by p_i^{d}, while N_1 and D present the number of objects and the dimension of the search space, respectively. The reaction force from object j to object i of dimension d at the specific time t is calculated as

$$F_{ij}^d(t) = G(t)\frac{M_i(t)M_j(t)}{\left\|P_i(t), P_j(t)\right\|_2}(p_j^d(t) - p_i^d(t)) \tag{9}$$

where $G(t)$ is the gravitational constant which is set to be G_0 at the beginning of the search process and is updated based on the Eq.(10) to ensure the performance of the search process at iteration t.

$$G(t) = G_0(t)e^{-\alpha t/T} \tag{10}$$

$M_i(t)$ and $M_j(t)$ are the mass of object i and object j respectively, which could be calculated according to Eq. (11) and Eq. (12)

$$M_i(t) = \frac{m_i(t)}{\sum_{j=1}^{N_1} m_j(t)} \tag{11}$$

$$m_i(t) = \frac{f_i(t) - f_{worst}(t)}{f_{best}(t) - f_{worst}(t)} \tag{12}$$

where $f_i(t)$ presents the value of the fitness of object i at time t, $f_{best}(t)$ and $f_{worst}(t)$ present the best and worst fitness respectively for the population at time t. For maximization problems, there is

$$f_{best}(t) = \max_{j\in\{1,2,\cdots N_1\}} f_j(t), f_{worst}(t) = \min_{j\in\{1,2,\cdots N_1\}} f_j(t) \tag{13}$$

TABLE 3. MSEs of the inverse model with different *N*.

N	3	4	5	6	7	8	9	10	11	12
MSEs ($\times 10^{-4}$)	3.32	3.08	3.17	2.93	2.86	2.68	2.65	2.71	2.96	2.83

The total reaction force from all of the other objects to the object i could be calculated as

$$F_i^d(t) = \sum_{j \neq i} rand_j F_{ij}^d(t) \tag{14}$$

where $rand_j$ is a random number with uniform distribution in the interval [0,1]. The acceleration of the object i is calculated according to Newton's second law of motion:

$$a_i^d(t) = \frac{F_i^d(t)}{M_i(t)} \tag{15}$$

then the velocity $v_i^d(t+1)$ and the position $p_i^d(t+1)$ of the object in the next iteration could be calculated as

$$v_i^d(t+1) = rand_i \times v_i^d(t) + a_i^d(t) \tag{16}$$

$$p_i^d(t+1) = p_i^d(t) + v_i^d(t+1) \tag{17}$$

where $rand_i$ is a random number with uniform distribution in the interval [0,1].

When GSA is employed to search the optimal value of the initial parameters of the BP neural network inverse model, the position of the object i could be encoded as

$$P_i = [w_{lh}, b_h, w_{hm}, b_m] \tag{18}$$

where $w_{lh} = \{w_{ji} | j = 1, \ldots, l, i = 1, \ldots, h\}$ is the weight set between the input layer neurons and the hidden layer neurons, $w_{hm} = \{w_{kj} | k = 1, \ldots, m, j = 1, \ldots, h\}$ is the weight set between the hidden layer neurons and the output layer neurons, b_h and b_m are the threshold vector of the hidden layer neurons and the output layer neurons, respectively.

Define fitness of the object i as the negative value of the mean square error (MSE) on the training data set

$$f_i = -\frac{1}{n} \sum_{i=1}^{n} (x_i - \hat{x})^2 \tag{19}$$

where n is the number of the samples in the training data set, x_i is the expected network output, and $\hat{x}$ is the actual network output.

When the search process is over, the standard BP algorithm is employed to train the network further based on the obtained optimal initial parameters. In this study, the maximum number of iterations of GSA is set to be 1000, while the size of the particle population N_1 is set to be different values to investigate the influence on the network's performance. When the network is directly trained by standard BP algorithm without the parameter optimization process based on GSA, the MSE on the test data set for 10 times of training is 2.94×10^{-4}, while the MSEs of the GSA-BP trained network on the test data set as well as the gain ratios are shown in Tab.5. It is known that the MSE gradually decreases with the increase of N_1 and no long changes when N_1 is greater than 50, and the GSA-BP trained network has obvious higher precision.

TABLE 4. MSEs of the inverse model with different activation functions.

Activation function in the hidden layer	Activation function in the output layer	MSEs ($\times 10^{-4}$)
sigmoid	purelin	2.65
sigmoid	tansig	2.73
sigmoid	sigmoid	2.82
tansig	purelin	2.85
tansig	tansig	2.93
tansig	sigmoid	2.87
purelin	purelin	7.98
purelin	tansig	6.64
purelin	sigmoid	5.65

TABLE 5. Performance of the network for with different N_1 on test data set.

N_1	10	20	30	40	50	60	100
MSEs ($\times 10^{-4}$)	0.54	0.42	0.36	0.34	0.33	0.33	0.33
Gain ratios	0.18	0.14	0.12	0.12	0.11	0.11	0.11

V. INVERSE CONTROL SCHEME DESIGN

Theoretically, the inverse model could be directly used as the controller for the original inverter system. That is, at the beginning of the k th control cycle, duty cycle $d(k)$ could be calculated by replacing the $u_o(k+1)$ in Fig.6 b) with $u_o^*(k+1)$, which is the reference value of u_o for $k+1$ th control cycle. However, this control scheme is quite sensitive to the accuracy of the inverse model, the minor error of the inverse model may cause poor control effect. Therefore, in this study, a pseudo-linear system is constructed by putting the expanded inverse model in series with the original system, then single-loop control is performed with PI controller, as shown in Fig.7. It's important to note that the input $u_o(k+1)$ in the inverse model is replaced by $u_{PI}(k)$, which is the output of the PI controller for k th control cycle.

Then, the control principle of the output voltage of BESS inverter could be regarded as Fig.8, in which the influence of inverse model error is equivalent to disturbance $D(s)$, and the performance of the system depends on the proportional gain k_p and integral gain k_i of the PI controller.

The closed-loop transfer function between the actual value and reference value of the output voltage is

$$G_C(s) = \frac{u_o(s)}{u_o^*(s)} = \frac{k_p s + k_i}{(1 + k_p)s + k_i} \tag{20}$$

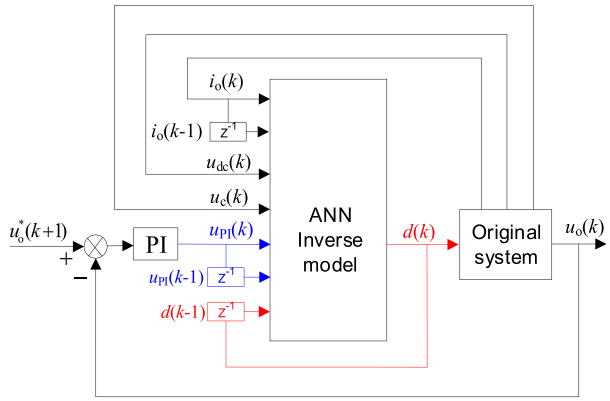

FIGURE 7. Single-loop control method with ANN inverse model.

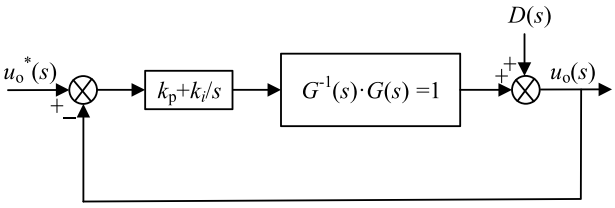

FIGURE 8. Control principle of the output voltage of BESS inverter.

while the closed-loop transfer function between the actual value of the output voltage and the disturbance is

$$G_N(s) = \frac{u_o(s)}{D(s)} = \frac{s}{(1+k_p)s + k_i} \tag{21}$$

It is known that the system is stable for the pole is distributed in the left half plane, and $k_p = 10$, $k_i = 320$ is adopted in this paper to achieve the good response to reference signal while the effective elimination of high frequency harmonics.

VI. SIMULATION EXPERIMENT

Based on the model of BESS inverter built with Matlab in Section IV, the presented single-loop control method with ANN inverse model is implemented, and the contrast simulation experiment with conventional PI control method is carried out for linear condition and nonlinear condition, respectively.

A. CONDITION 1: LINEAR EQUIVALENT LOAD, A 2.5KW RESISTOR TYPE LOAD.

As seen in Fig.9, both control methods could achieve satisfactory control results that the BESS inverter output voltage u_o is in sinusoidal form. However, total harmonic distortion rate (THD) of the conventional PI control method is 3.94%, while THD of the presented control method achieves a lower 2.25%; The maximum over shoot at voltage peak is 1.2V for conventional PI control method, while it is 0.3V for the presented control method. It is indicated that the presented method has a better voltage waveform quality than the conventional PI control method.

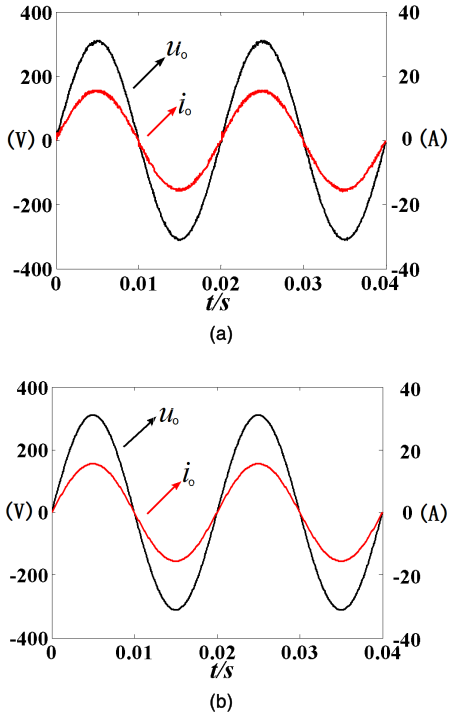

FIGURE 9. Output waveforms for different control methods with resistor type load. a) Waveforms for the conventional PI control method; b) waveforms for the presented control method.

B. CONDITION 2: NONLINEAR EQUIVALENT LOAD, A 2.5KW RECTIFIER TYPE LOAD. (CONDUCTING ANGLE IS 60°)

As seen in Fig.10 a), when rectifier type load turns on and turns off, dramatically oscillation of BESS inverter output voltage u_o happens for the conventional PI control method, and the THD is 6.24%. While in Fig.10 b), when rectifier type load turns on and turns off, a much smaller oscillation of BESS inverter output voltage u_o happens for the presented control method, and the THD is 3.87%. The maximum over shoot of the regulating process is 147V for conventional PI control method, while it is 35V for the presented control method. The average settling time of the regulating process is 0.62ms, while it is 0.23ms for the presented control method. It is indicated that the presented method has a more robust characteristic than conventional PI control method for disturbance of output current.

C. CONDITION 3: NONLINEAR EQUIVALENT LOAD, LOAD SWITCHING.

At first, the inverter works with full load, then switches to no load at the moment $t = 0.015$s and switches to full load again at the moment $t = 0.043$s. Fig.11 a) shows waveforms of the output voltage and output current when the inverter is controlled with conventional PI control method, it is known that, when switches to no load from full load at the moment $t = 0.015$s, both the inverter output voltage and output current oscillate obviously, the over shoot of the output

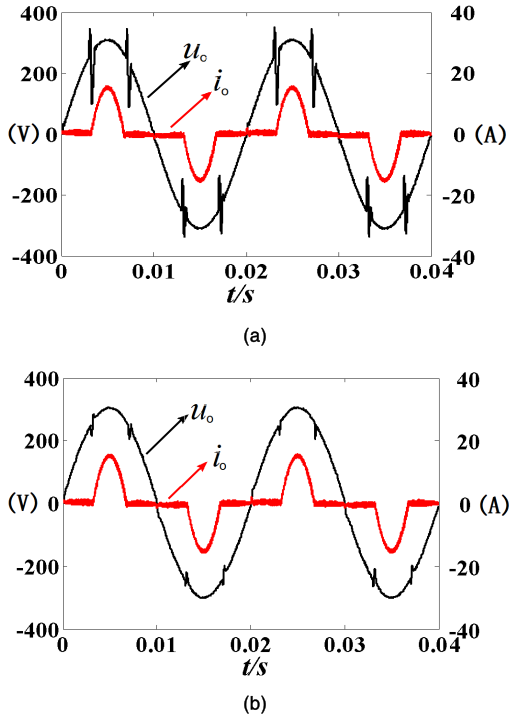

FIGURE 10. Output waveforms for different control methods with rectifier type load. a) Waveforms for the conventional PI control method; b) waveforms for the presented control method.

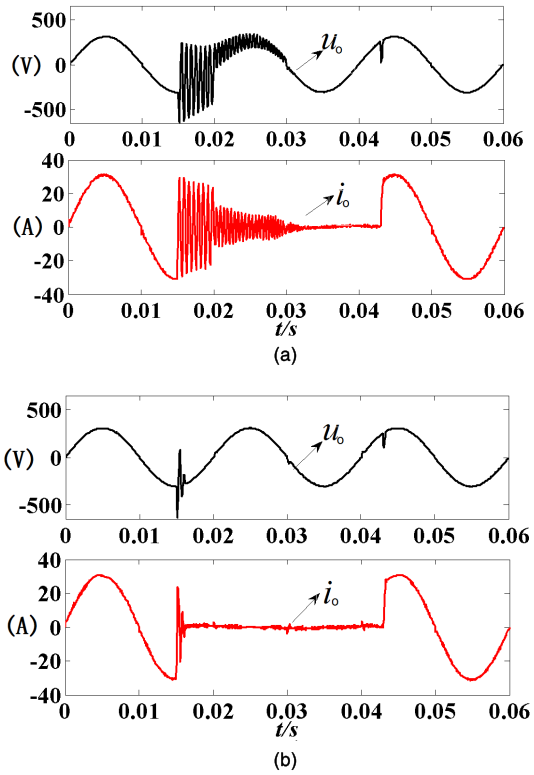

FIGURE 11. Output waveforms for different control methods with load switching. a) Waveforms for the conventional PI control method; b) waveforms for the presented control method.

voltage is 239V and the settling time of the regulating process is 15.26ms; when switch to full load again at the moment $t = 0.043$s, the output current increases suddenly and the output voltage is obviously pulled down, the over shoot of the output voltage is 230V and the settling time of the regulating process is 0.48ms.

Fig.11 b) shows waveforms of the output voltage and output current when the inverter is controlled with presented control method, it is known that, at the moment $t = 0.015$s, both the inverter output voltage and output current oscillate slightly, the over shoot of the output voltage is 77V and the settling time of the regulating process is 1.64ms; at the moment $t = 0.043$s, the output current increases suddenly and the output voltage is also pulled down but with smaller amplitude, the over shoot of the output voltage is 139V and the settling time of the regulating process is 0.42ms. It is indicated that the presented control method has better adaptability to load switching than the conventional PI control method.

VII. PROTOTYPE EXPERIMENT

In order to verify the performance of the presented control method, a BESS inverter prototype which mainly consists of Microprocessor, FPGA, Intelligent power module (IPM), and LCL filter is implemented, as shown in Fig.12, while the parameters of the hardware setup are shown in Tab.6. The Microprocessor is responsible for signal sampling, while FPGA is to achieve the real-time calculation of the ANN inverse model for every control cycle. Because FPGA can

TABLE 6. Parameters of the hardware setup.

Parameter name	Parameter value
Microprocessor	dsPIC33FJ16GS504
FPGA	EP4CE22F17
Intelligent power module (IPM)	PM100CG1B120
Voltage sensor	LV25-1000
Current sensor	LA50-S/SP1
Gate drive optocoupler	HCPL-4504
Oscilloscope	Aglient 54645A
LCL Filter inductance L_1	4.7 mH
LCL Filter capacity C	6.8 uF
LCL Filter inductance L_2	1.2 mH

not directly take index computation, one important problem is how to calculate the e^x item for sigmoid function

$$y = f(x) = \frac{1}{1+e^{-x}} = \frac{e^x}{e^x+1} \tag{22}$$

In this study, Taylor series expansion method is adopted to approximately calculate the e^x item as

$$e^x \approx 1 + x + \frac{x^2}{2!} + \frac{x^3}{3!} + \ldots \frac{x^N}{N!} \tag{23}$$

where N is the expansion orders. The higher the expansion orders is, the more accurate the calculated result is. However, higher expansion orders needs more calculation consumption

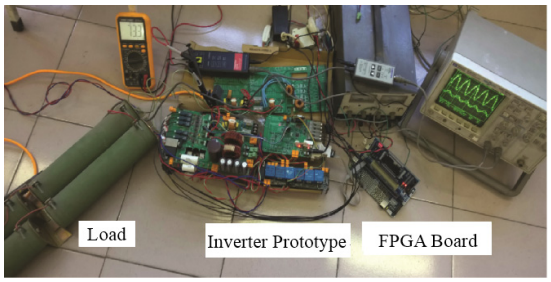

FIGURE 12. Prototype of BESS inverter.

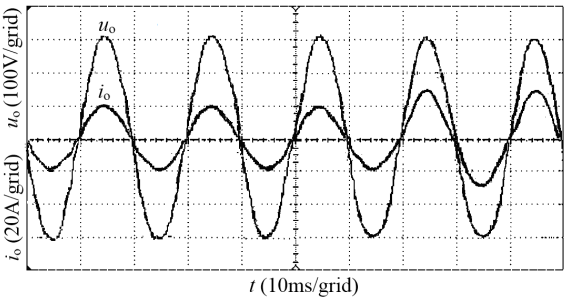

FIGURE 13. Output waveforms for the presented control method when resistor type load is increased.

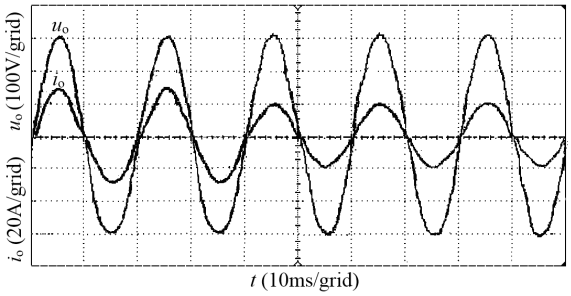

FIGURE 14. Output waveforms for the presented control method when resistor type load is decreased.

of FPGA. In this study, the expansion orders is chosen to be 10, by which the maximum absolute error of the calculated sigmoid function is 2.4910^{-4} when x is between [-10,10].

Considering that the working condition of load disturbance is more challenging, the prototype experiment are carried out for loading switching and rectifier load respectively.

A. CONDITION 1: LOAD SWITCHING, INCLUDING LOAD INCREASING AND LOAD DECREASING.

Adjust the BESS port voltage u_{dc} to be 400V, the performance of BESS inverter for load increasing and decreasing is shown in Fig.13 and Fig.14 respectively. In Fig.13, the equivalent load is 3 kW resistive load at the moment t =0s and increases to 4.5kW at the moment t = 0.07s; on the contrary, in Fig.14, the equivalent load is 4.5 kW resistive load at the moment t = 0s and decreases to 3kW at the moment t = 0.04s. During load switching, there is no obvious waveform distortion for output voltage u_o, which indicate that the presented

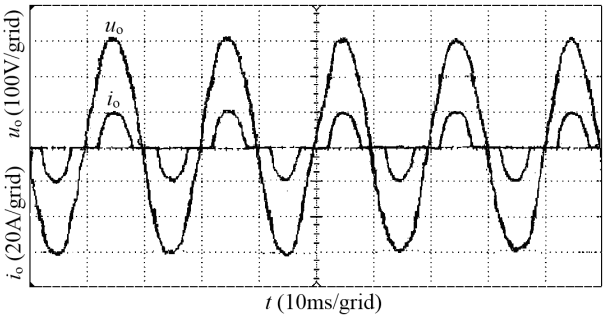

FIGURE 15. Output waveforms for the presented control method with rectifier type load.

TABLE 7. Voltage harmonics for different BESS port voltage.

BESS port voltage(V)	THD of voltage (%)
355	4.71
382	4.56
415	4.32
438	3.96

control method has robust characteristics for loading switching. The THDs of voltage waveform are 3.16% and 3.64% respectively for steady conditions of 3kW resistive load and 4.5kW resistive load, which quite agrees with the result of simulation.

B. CONDITION 2: NONLINEAR EQUIVALENT LOAD, A 3KW RECTIFIER TYPE LOAD. (CONDUCTING ANGLE IS 45°)

Adjust the BESS port voltage u_{dc} to be 400V, the performance of ESS inverter for rectifier type load is shown in Fig.15. It is known that the waveform of inverter output voltage u_o has a high degree of sine, and the THD of voltage waveform is 4.43%.

In order to verify the adaptive capability of the presented control method to BESS port voltage, set the BESS with different SOC, and calculate the THD of the voltage waveform with 3kW rectifier type load (conducting angle is 45°), as shown in Tab.7. It is known that when BESS port voltage changes, the THD of the voltage waveform varies in quite small scope and meets the international standards (<5%), which indicates that the presented control method could overcome the disturbance of the BESS port voltage. In addition, the increasing of BESS port voltage corresponds to the decreasing of THD, the reason is that the BESS port voltage u_{dc} is in the numerator of the Eq. (6), which directly affects the gain of the open-loop transfer function, while higher open-loop gain will benefit the reduction of steady-state error and settling time for the closed-loop system according to the control theory.

VIII. CONCLUSION

An expanded inverse model control method for the output voltage of the BESS inverter in stand-alone micro-grid is

proposed in this study. Based on the analysis of main factors affecting the inverter output voltage, an expanded inverse model of BESS inverter is established using BP neural network, and the gravity search algorithm is employed to search the optimal value of the network's initial parameters to avoid falling into local optimality in the training process. A pseudo linear system is constructed by putting the expanded inverse model in series with the original system, and then PI controller is adopted to realize the single-loop control of the output voltage. Both simulation experiment results and prototype experiment results show that the proposed expanded inverse model control method has a strong capability of disturbance rejection and could ensure the high power quality.

The future work of this study mainly includes two aspects: first, more inverter operation data under different load conditions would be collected to enrich the training sample data of the inverse model and improve the accuracy of the inverse model; second, the on-line training and real-time updating of the inverse model would be considered on the inverter prototype so as to further improve the control effect of the output voltage.

REFERENCES

[1] D. E. Olivares, A. Mehrizi-Sani, A. H. Etemadi, C. A. Cañizares, R. Iravani, M. Kazerani, A. H. Hajimiragha, O. Gomis-Bellmunt, M. Saeedifard, R. Palma-Behnke, and G. A. Jiménez-Estévez, "Trends in microgrid control," *IEEE Trans. Smart Grid*, vol. 5, no. 4, pp. 1905–1919, Jul. 2014, doi: 10.1109/ TSG.2013.2295514.

[2] E. Mengelkamp, G. Johannes, and K. Rock, "Designing microgrid energy markets : A case study: The Brooklyn Microgrid," *Appl. Energy*, vol. 210, pp. 870–880, Jan. 2018, doi: 10.1016/j.apenergy.2017.06.054.

[3] W. Liu, C. Liu, Y. Lin, L. Ma, K. Bai, and Y. Wu, "Optimal scheduling of residential microgrids considering virtual energy storage system," *Energies*, vol. 11, no. 4, p. 942, Apr. 2018, doi: 10.3390/en11040942.

[4] J. Zhou, S. Kim, H. Zhang, Q. Sun, and R. Han, "Consensus–based distributed control for accurate reactive, harmonic, and imbalance power sharing in microgrids," *IEEE Trans. Smart Grid*, vol. 9, no. 4, pp. 2453–2467, Jul. 2018, doi: 10.1109/tsg.2016.2613143.

[5] M. Savaghebi, A. Jalilian, J. C. Vasquez, and J. M. Guerrero, "Autonomous voltage unbalance compensation in an islanded droop–controlled microgrid," *IEEE Trans. Ind. Electron.*, vol. 60, no. 4, pp. 1390–1402, Apr. 2013, doi: 10.1109/tie.2012.2185914.

[6] A. H. Etemadi and R. Iravani, "Overcurrent and overload protection of directly voltage–controlled distributed resources in a microgrid," *IEEE Trans. Ind. Electron.*, vol. 60, no. 12, pp. 5629–5638, Dec. 2013, doi: 10.1109/tie.2012.2229680.

[7] W. Liu, C. Liu, Y. Lin, K. Bai, L. Ma, and W. Chen, "Multi–objective optimal scheduling method for a grid–connected redundant residential microgrid," *Processes*, vol. 7, no. 5, p. 296, May 2019, doi: 10.3390/pr7050296.

[8] L. Yang, N. Tai, C. Fan, and Y. Meng, "Energy regulating and fluctuation stabilizing by air source heat pump and battery energy storage system in microgrid," *Renew. Energy*, vol. 95, pp. 202–212, Sep. 2016, doi: 10.1016/j.renene.2016.04.019.

[9] J. Quesada, R. Sebastián, M. Castro, and J. Sainz, "Control of inverters in a low voltage microgrid with distributed battery energy storage. Part I: Primary control," *Electr. Power Syst. Res.*, vol. 114, pp. 126–135, Sep. 2014, doi: 10.1016/j.epsr.2013.11.023.

[10] X. Quan, X. Dou, Z. Wu, M. Hu, and J. Yuan, "Harmonic voltage resonant compensation control of a three-phase inverter for battery energy storage systems applied in isolated microgrid," *Electr. Power Syst. Res.*, vol. 131, pp. 205–217, Feb. 2016, doi: 10.1016/j.epsr.2015.10.010.

[11] J. Khajesalehi, M. Hamzeh, K. Sheshyekani, and E. Afjei, "Modeling and control of quasi Z-source inverters for parallel operation of battery energy storage systems: Application to microgrids," *Electr. Power Syst. Res.*, vol. 125, pp. 164–173, Aug. 2015, doi: 10.1016/j.epsr.2015.04.004.

[12] N. Altin and İ. Sefa, "dSPACE based adaptive neuro-fuzzy controller of grid interactive inverter," *Energy Convers. Manage.*, vol. 56, pp. 130–139, Apr. 2012, doi: 10.1016/j.enconman.2011.11.017.

[13] M. Calais, V. G. Agelidis, and M. S. Dymond, "A cascaded inverter for transformerless single-phase grid-connected photovoltaic systems," *Renew. Energy*, vol. 22, nos. 1–3, pp. 255–262, Jan. 2001, doi: 10.1016/s0960-1481(00)00069-0.

[14] C. Attaianese, M. Di Monaco, and G. Tomasso, "High performance digital hysteresis control for single source cascaded inverters," *IEEE Trans. Ind. Informat.*, vol. 9, no. 2, pp. 620–629, May 2013, doi: 10.1109/tii.2012.2221130.

[15] K.-S. Kim, Y.-H. Cho, H.-S. Kim, T.-S. Kang, and S.-K. Hong, "Characteristic comparison between PI and hysteresis voltage control of high voltage unidirectional inverter for piezoelectric load using FPGA," *Trans. Korean Inst. Elect. Eng.*, vol. 66, no. 1, pp. 48–54, Jan. 2017, doi: 10.5370/kiee.2017.66.1.48.

[16] M. Monfared and H. Rastegar, "Design and experimental verification of a dead beat power control strategy for low cost three phase PWM converters," *Int. J. Electr. Power Energy Syst.*, vol. 42, no. 1, pp. 418–425, Nov. 2012, doi: 10.1016/j.ijepes.2012.04.044.

[17] C. Cheng, H. Nian, X. Wang, and D. Sun, "Dead-beat predictive direct power control of voltage source inverters with optimised switching patterns," *IET Power Electron.*, vol. 10, no. 12, pp. 1438–1451, Oct. 2017, doi: 10.1049/iet-pel.2016.0869.

[18] H. Komurcugil, N. Altin, S. Ozdemir, and I. Sefa, "Lyapunov–function and proportional-resonant-based control strategy for single–phase grid–connected VSI with LCL filter," *IEEE Trans. Ind. Electron.*, vol. 63, no. 5, pp. 2838–2849, May 2016, doi: 10.1109/tie.2015.2510984.

[19] C. Xia, Z. Wang, T. Shi, and X. He, "An improved control strategy of triple line–voltage cascaded voltage source converter based on proportional-resonant controller," *IEEE Trans. Ind. Electron.*, vol. 60, no. 7, pp. 2894–2908, Jul. 2013, doi: 10.1109/tie.2012.2222854.

[20] B. Widrow and E. Walach. *Adaptive Inverse Control*. Upper Saddle River, NJ, USA: Prentice-Hall, 1996.

[21] X. Dai, *Multivariable Nonlinear Neural Network Inverse System Control Method*. Beijing, China: Science, 2005.

[22] K. Y. Lee, J. H. Van Sickel, J. A. Hoffman, W.-H. Jung, and S.-H. Kim, "Controller design for a large–scale ultrasupercritical once–through boiler power plant," *IEEE Trans. Energy Convers.*, vol. 25, no. 4, pp. 1063–1070, Dec. 2010, doi: 10.1109/tec.2010.2060488.

[23] L. Ma, K. Y. Lee, and Z. Wang, "Intelligent coordinated controller design for a 600MW supercritical boiler unit based on expanded-structure neural network inverse models," *Control Eng. Pract.*, vol. 53, pp. 194–201, Aug. 2016, doi: 10.1016/j.conengprac.2015.09.002.

[24] J. Labus, J. Hernández, J. Bruno, and A. Coronas, "Inverse neural network based control strategy for absorption chillers," *Renew. Energy*, vol. 39, no. 1, pp. 471–482, Mar. 2012, doi: 10.1016/j.renene.2011.08.036.

[25] S. Xing, J. Ju, and J. Xing, "Research on hot-rolling steel products quality control based on BP neural network inverse model," *Neural Comput. Appl.*, vol. 31, no. 5, pp. 1577–1584, May 2019, doi: 10.1007/s00521-018-3547-5.

[26] L. Chen, C. Zhu, Z. Zhong, M. Sun, and W. Zhao, "Internal model control for the AMB high-speed flywheel rotor system based on modal separation and inverse system method," *IET Electr. Power Appl.*, vol. 13, no. 3, pp. 349–358, Mar. 2019, doi: 10.1049/iet-epa.2018.5646.

[27] W. Liu, H. Zhang, C. Liu, Y. Lin, L. Ma, and W. Chen, "Energy storage inverter control based on neural network inverse model," in *Proc. IEEE Int. Conf. Inf. Autom.*, Lijiang, China, Aug. 2015, pp. 3032–3036.

[28] R. Wang, Q. Sun, D. Ma, and Z. Liu, "The small–signal stability analysis of the droop–controlled converter in electromagnetic timescale," *IEEE Trans. Sustain. Energy*, vol. 10, no. 3, pp. 1459–1469, Jul. 2019, doi: 10.1109/tste.2019.2894633.

[29] M. Liserre, F. Blaabjerg, and S. Hansen, "Design and control of an LCL-filter-based three–phase active rectifier," *IEEE Trans. Ind. Appl.*, vol. 41, no. 5, pp. 1281–1291, Sep. 2005.

[30] M. Liserre, A. Dell'aquila, and F. Blaabjerg, "Design and control of a three-phase active rectifier under non-ideal operating conditions," in *Proc. Conf. Rec. IEEE Ind. Appl. Conf. 37th IAS Annu. Meeting*, Pittsburgh, PA, USA, Jun. 2003, pp. 1181–1188, doi: 10.1109/ias.2002.1042708.

[31] M. Chen, W. Yao, and Z. Qiu, "Analysis of inverter characteristics with rectifier load using a nonlinear rectifier model," *Proc. CSEE*, vol. 28, pp. 44–48, May 2008.

[32] E. Rashedi, H. Nezamabadi-Pour, and S. Saryazdi, "GSA: A gravitational search algorithm," *Inf. Sci.*, vol. 179, no. 13, pp. 2232–2248, Jun. 2009, doi: 10.1016/j.ins.2009.03.004.

XINGWU WANG received the B.S. degree in computer science and technology and the M.S. degree in automation from North China Electric Power University (NCEPU), Baoding, China, in 1997 and 2005, respectively, where he is currently pursuing the Ph.D. degree in control theory and control engineering.

Since 2013, he has been a Senior Engineer with the Department of Automation, NCEPU. His research interests include control technology in renewable energy generation and electrical drive.

YONGJUN LIN received the B.S. and M.S. degrees in measurement and automation and the Ph.D. degree in thermal power engineering from North China Electric Power University (NCEPU), Baoding, China, in 1986, 1989, and 2002, respectively.

He is currently a Professor with the Department of Automation, NCEPU. His research interests include the application of embedded technology and control technology in micro-grids.

BINGSHU WANG received the M.S. degree in thermal power engineering from North China Electric Power University (NCEPU), Baoding, China, in 1981.

He is currently a Professor with the Department of Automation, School of Control and Computer Engineering, NCEPU. His research interests include industrial process simulation and control, large capacity motor speed and control technology, and application of intelligent technologies in power plant control and diagnosis.

WEILIANG LIU received the B.S. degree in automation from North China Electric Power University (NCEPU), Baoding, China, in 2005, the M.S. degree in system engineering from Xi'an Jiaotong University (XJTU), Xi'an, China, in 2008, and the Ph.D. degree in control theory and control engineering from NCEPU, in 2019.

Since 2008, he has been a Lecturer with the Department of Automation, NCEPU. His research interests include control technology in renewable energy generation and micro-grids.